Chemistry–A European Journal
Research Article
doi.org/10.1002/chem.202201884
Chemistry Europe
European Chemical Societies Publishing
www.chemeurj.org

Flexible Alkylene Bridges as a Tool To Engineer Crystal Distyrylbenzene Structures Enabling Highly Fluorescent Monomeric Emission

Yoshimichi Shimomura,[a] Kazunobu Igawa,[b] Shunsuke Sasaki,[c] Noritaka Sakakibara,[d] Raita Goseki,[e] and Gen-ichi Konishi*[a, f]

Abstract: To design ultrabright fluorescent solid dyes, a crystal engineering strategy that enables monomeric emission by blocking intermolecular electronic interactions is required. We introduced propylene moieties to distyrylbenzene (DSB) as bridges between the phenyl rings either side of its C=C bonds. The bridged DSB derivatives formed compact crystals that emit colors similar to those of the same molecules in dilute solution, with high quantum yields. The introduction of flexible seven-membered rings to the DSB core produced moderate distortion and steric hindrance in the DSB π-plane. However, owing to this strategy, it was possible to control the molecular arrangement with almost no decrease in the crystal density, and intermolecular electronic interactions were suppressed. The bridged DSB crystal structure differs from other DSB derivative structures; thus, bridging affords access to novel crystalline systems. This design strategy has important implications in many fields and is more effective than the conventional photofunctional molecular crystal design strategies.

Introduction

Recently, ultrabright solid-state fluorescent materials containing organic dyes have been applied to the fabrication of organic light-emitting devices (OLEDs)[1] and nanoparticles,[2] as well as for circularly polarized luminescence experiments,[3] in bioimaging,[4] and for lasers.[5] The wide applicability of these materials is a function of their versatility, in terms of molecular design, and excellent processability. Optimization of the luminous efficiencies, emission colors, crystallinities, and molecular orientations of solid-state fluorescent dyes are required for the design of advanced OLEDs. At present, the challenges associated with these devices are as follows. 1) Developing fluorescent dyes that exhibit high luminescence efficiencies without concentration quenching in their solid states is essential.[6] J-aggregates are fluorescent dyes that exhibit strong solid-state luminescence; however, the fluorescence wavelengths of their aggregated forms are different with respect to the monomer emissions.[7] These simple systems function based on external shielding by bulky substituents (site isolation effect),[8] or by preventing association through hydrogen bonding or ion-pair formation.[9] Another type of system-aggregation-induced emission (AIE) luminogens (AIEgens) has been investigated.[10] However, in these systems, the dye molecules are large. Small dye molecules and crystals with small free volumes are desired for electronic device applications.[11] 2) Predicting solid-state fluorescence spectra from dilute-solution or distributed-matrix fluorescence spectra is challenging. Numerous organic dyes form aggregates of ≥ 2 molecules in the excited state,[12] and the fluorescence wavelengths often change due to intermolecular electronic interactions. Therefore, monomeric emissive dyes with high quantum yields possess advantages in the field of materials design. 3) To obtain monomeric emission, controlling the dye arrangement is essential. Methodologies based on arranging molecular π-skeletons appropriately such that dye molecules without bulky substituents (without increased free volume) exhibit monomeric

[a] *Y. Shimomura, Prof. Dr. G.-i. Konishi*
Department of Chemical Science and Engineering
Tokyo Institute of Technology
2-12-1 O-okayama, Meguro-ku, 152-8552 Tokyo (Japan)
E-mail: konishi.g.aa@m.titech.ac.jp

[b] *Prof. Dr. K. Igawa*
Institute for Materials Chemistry and Engineering
Kyushu University
6-1 Kasuga-koen, Kasuga, 816-8580 Fukuoka (Japan)

[c] *Dr. S. Sasaki*
Université de Nantes, CNRS
Institut des Matériaux Jean Rouxel, IMN
F-44000 Nantes (France)

[d] *Dr. N. Sakakibara*
Department of Chemistry, Tokyo Institute of Technology
2-12-1 O-okayama, Meguro-ku, 152-8552 Tokyo (Japan)

[e] *Prof. Dr. R. Goseki*
Department of Applied Chemistry, Kogakuin University
Nakano-machi, Hachioji-shi, 192-0015 Tokyo (Japan)

[f] *Prof. Dr. G.-i. Konishi*
PRESTO "Element Strategy"
Japan Science and Technology Agency (JST)
Kawaguchi, Saitama 332-0012, (Japan)

Supporting information for this article is available on the WWW under https://doi.org/10.1002/chem.202201884

emission remain underdeveloped. Therefore, novel functional groups must be attached to the π-electron framework to control the crystalline system. In addition, introducing a new functional group into an existing π-electronic compound may afford a different crystalline structure. Increased diversity in crystal engineering is important for the development of material design strategies.

In this study, we prepared highly fluorescent monomeric emissive dyes, di-bridged distyrylbenzenes (DSBs), DBDB[7]s, with highly dense crystalline structures, by introducing flexible cyclic structures into π-conjugated DSB systems. We propose a new crystal engineering method to control luminescence and electronic properties in which simple alkylene bridges are introduced to π-electron compounds. We designed DBDB[7]s with reference to a well-known fluorescent dye, viz., DSB.[13,14] The DBDB[7] structures include two seven-membered rings with C=C bonds bridged loosely by propylene chains, which are much smaller functional groups than those studied in previous reports (Figure 1). This structure design suppressed intermolecular electronic interactions without distancing the chromophores – a typical result of steric-hindrance-based intermolecular-interaction-suppression strategies. This result is in stark contrast with DSB-bearing H-aggregates[15] – the DBDB[**7**]s reported herein underwent only very minor emission-wavelength shifts. Moreover, the DBDB[**7**]s exhibit AIE properties, controllable fluorescence emission, and are not mechanochromic.

Results and Discussion

In this study, we classified DSB analogs into two categories dependent on their photophysical properties: Category A is represented by DBDB[7] and structural homologues, whereas Category B includes not only DSB but also other related dyes that exhibit similar photophysical properties. DSB, PPB, and DSDMB have been previously reported.[15–17] We classified the novel compound DBDB[6] as a Category B DSB owing to its similarity to DSBs in terms of their photophysical properties. We synthesized DSBs and bridged DSBs (DBDB[6] and DBDB[7]s); detailed synthetic methods[18] are described in the Supporting Information. Previously, we proposed the concept of bridged stilbenes for AIEgen design.[19] In that case, a flexible ring structure mechanically controlled the accessibility of the configuration taken during the process of quenching the excited-state stilbene. Compared to the melting point of 4-phenylstilbene, that of bridged 4-phenylstilbene (8-([1,1′-biphenyl]-4-yl)-6,7-dihydro-5*H*-benzo[7]annulene)[19] was decreased by 120 °C, and there was not a significant increase in the free volume in the crystal. This result inspired the design of the new dyes presented herein. Similar results were obtained for curved nanographene[20] and carbon nanotubes,[21] whose solubility was improved by introducing a seven-membered ring.

Photophysical properties

The photophysical properties, that is, the molar absorption coefficient (ε), the maximum absorption wavelength (λ_{abs}), maximum fluorescence emission wavelength (λ_{fl}), and quantum yield Φ_{fl}, in both tetrahydrofuran (THF) and the solid-state, are listed in Table 1. Although DSBs have been reported previously,[15–17] a systematic study of the photophysical properties of DSBs, in both dilute solution and the solid state, has not been reported. Therefore, we synthesized DSBs to perform a study of this type. For example, for DSB, λ_{abs}, λ_{fl}, and Φ were measured in dilute dichloromethane and in a single crystal; for PPB, λ_{abs} and λ_{fl} were measured in dilute THF and in the aggregated form; and for DSDMB, λ_{abs} was measured in dilute chloroform only.

Dilute solutions of DSB, DSDMB, and DBDB[6] in THF exhibit similar λ_{abs} of ~350 nm and Φ_{THF} of ~0.90. Meanwhile, PPB, which contains methyl groups at the C=C bonds, exhibits a ~40 nm blue-shifted λ_{abs} of 314 nm and nearly quenched fluorescence with a Φ_{THF} of 0.01. DBDB[7], with a flexible propylene bridge, also exhibits a blue-shifted λ_{abs} (320 nm) and a low Φ_{THF} (0.11). Moreover, introducing methyl groups at the central benzene or bridging C=C bonds results in further blue-shifting of λ_{abs} (DBDMDB[7]: λ_{abs} = 273 nm, DBαMDB[7]: λ_{abs} = 284 nm), with Φ_{THF} values of < 1 %.[22] The value of ε depends on the planarity of the molecular structure and decreases in the following order: structures without cyclic moieties > six-membered ring > seven-membered ring > methyl-substituted C=C; this order correlates with increasing π-conjugation length and destabilization of the Franck–Condon (FC) energy at the excited state. All the compounds, except DBαMDB[7], 5DBαMDB[7], and *t*BuDBαMDB[7] (these had no emissions; we refer to these as the DBαMDB[**7**]s compounds in this report), exhibited similar

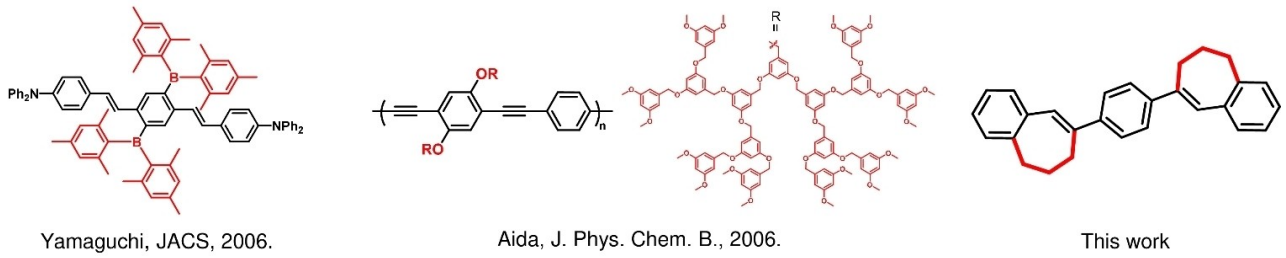

Figure 1. Previously reported organic dyes that exhibit solid-state fluorescence[8a,b] and the solid-state-fluorescing organic dye designed in this work. Functional groups are shown in red.

Table 1. Photophysical properties of DSBs, DBDB[6], and DBDB[7]s in THF and their solid states.

	ε [M cm^{-2}]	λ_{abs}[n] [nm]	$\lambda_{fl,THF}$[a] [nm]	$\lambda_{fl,solid}$ [nm]	Φ_{THF}[a]	Φ_{solid}	τ_{THF}[f] [ns]	τ_{solid} [ns]	$k_{r,THF}$ [10^8 s^{-1}]	$k_{r,solid}$ [10^8 s^{-1}]	$k_{nr,THF}$ [10^8 s^{-1}]	$k_{nr,solid}$ [10^8 s^{-1}]
DSB	59000	355	411	465[b]	0.89	0.53[c]	1.45[h]	1.76[fi]	6.14[l]	3.01[m]	0.76[l]	2.67[m]
DSDMB	45000	353	426	451[c]	0.91	0.45[c]	1.54	–[j]	5.91	–	0.58	–
PPB	36000	314	411	456[d]	0.01	0.96[b]	–	1.36[f]	–	6.99	–	0.37
DBDB[6]	44000	349	423	451[b]	>0.99	0.70[b]	1.40	3.92[f]	7.07	1.79	0.07	0.26
DBDB[7]	36000	320	408	400[d]	0.11	0.94[b]	0.21	1.61[f]	5.24	5.71	42.4	0.50
DBDMDB[7]	40000	273	392	382[e]	0.01	0.93[e]	–	–[k]	–	–	–	–
DBαMDB[7]	28000	284	–	413[d]	<0.01	>0.99[b]	–	1.21[f]	–	8.18	–	0.08
5DBαMDB[7]	31000	286	–	407[d]	<0.01	>0.99[b]	–	1.00[f]	–	9.90	–	0.10
*t*BuDBαMDB[7]	26000	283	–	365[e]	<0.01	0.84[d]	–	–[g,j,k]	–	–	–	–

Excitation wavelength: [a] max λ_{abs}, [b] 370 nm, [c] 400 nm, [d] 330 nm, [e] 300 nm, [f] 379 nm, and [g] 269 nm. [h] Only τ_2 is shown as its contribution to the overall decay is 91%. τ_1 = 0.74 ns (9%). [i] Only τ_1 is shown as its contribution to the overall decay is 93%. τ_2 = 3.92 ns (7%). [j] Two components. DSDMB: 0.82 ns (63%) and 1.67 ns (37%); *t*BuDBαMDB[7]: 0.13 ns (32%) and 1.74 ns (68%). [k] As we did not have the proper wavelength cutting filter or LED laser, it was not possible to obtain these values for DBDMDB[7], and the result for *t*BuDBαMDB[7] might be inaccurate. [l] Calculated from τ_2. [m] Calculated from τ_1. [n] Dilute THF solution. The absorption spectra of the solid-state compounds were measured by the diffuse-reflection method (Figure S3).

fluorescence maxima $\lambda_{fl,THF}$ (392–426 nm). This also implies that their lowest singlet excited states have similar geometries (S1 min structures), regardless of the existence of a bridged structure or of the introduction of methyl groups at the C=C bonds.

We calculated the radiative and non-radiative transition rates (k_r and k_{nr}, respectively) of DSB, DSDMB, DBDB[6], and DBDB[7] in THF solutions. In the case of DSB, fluorescence lifetimes (τ) of both the solution and solid have two components. However, since the contribution of one of the lifetime components was far more significant, that value was used to approximate the rate constant. All the k_r values were similar (5.2–7.1 × 10^8 s^{-1}), but for DBDB[7], k_{nr} is more than 50-fold larger than those of the other compounds (Table 1). The fluorescence quenching of the DBDB[**7**]s in solution occurs through pyramidal structures due to cleavage of π-conjugation of the C=C bonds, similar to the situation in stilbene derivatives.[19,23] In addition, the conjugation lengths shorten, and the FC energies are destabilized.

This fact explains the low ε, λ_{abs}, and Φ_{THF} values of the DBDB[7]s and PPB. The photophysical properties of DSDMB and DBDB[6] are similar to those of DSB, as the planarity of the DSB structure is preserved in these molecules.

The quantum yields of DSB, DSDMB, and DBDB[6] are higher in dilute solution than in the solid state, which is typical behavior for dyes exhibiting concentration quenching. In contrast, PPB and the DBDB[7]s, which exhibit weak fluorescence in dilute solution, display solid-state Φs values that are >0.80 higher than those in solution. The $\lambda_{fl,solid}$ values of the DSBs are red-shifted by approximately 50 nm with respect to the corresponding $\lambda_{fl,THF}$ values, whereas those of the DBDB[7]s, except *t*BuDBαMDB[7], are approximately 400 nm. The $\lambda_{fl,solid}$ value of *t*BuDBαMDB[7] is 365 nm, which is 40 nm shorter than those of the other DBDB[7]s. The fluorescence lifetimes of the solids (τ_{solid}) are ≤2.0 ns for all the compounds except DBDB[6] (τ_{solid} = 3.92 ns). Bridged DSB derivatives cannot form excimers. Between the dilute THF solution and solid states, the k_r values differ by >0.31 ns^{-1} for DSB and DBDB[6], whereas this difference is only 0.05 ns^{-1} for DBDB[7]. We analyzed the differences between the fluorescence properties in solution and the solid state for the two categories shown in Figure 2.

Category A

In general, efficient solid-state fluorescence usually occurs for aggregates, such as J-aggregates,[7] or excimers,[24] or solid-state monomeric emission can be efficient.[6] For DBDB[7], DBDMDB[7], and DBαMDB[7], the change in the fluorescence wavelength is minor (wavelength shift, <10 nm; Figure 3a), and

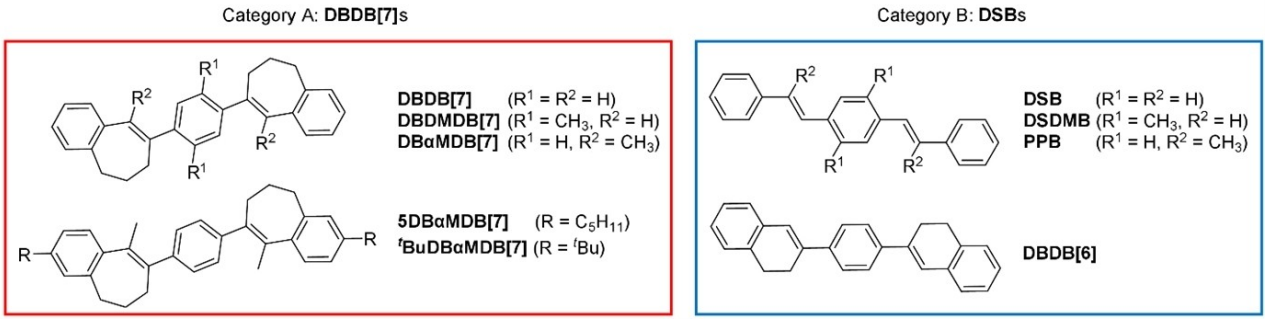

Figure 2. Structures of the DSBs, DBDB[6], and DBDB[7]s classified into two categories.

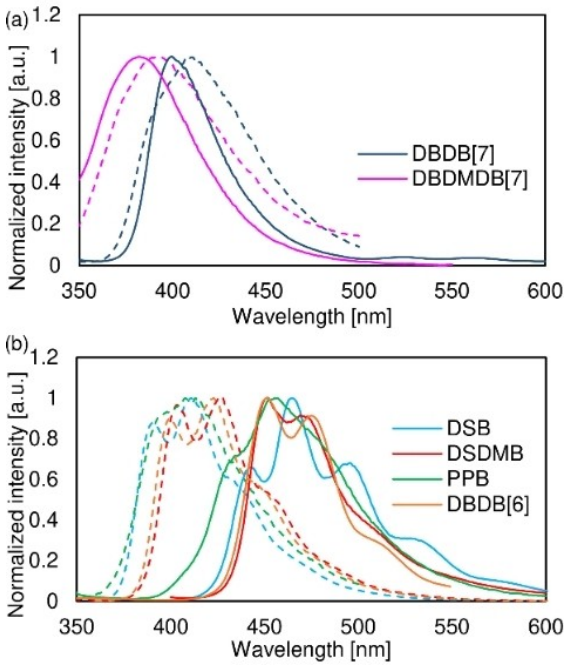

Figure 3. Fluorescence spectra of a) DBDB[7]B, DBDMDB[7], and b) DSBs in dilute THF (dashed lines) and in the solid state (solid lines).

the quantum yield is >0.8 higher in the solid state than in solution. Although new band structures were observed for these dyes, the changes were small; therefore, the fluorescence properties are comparable to those of monomeric luminescence.

DBDB[7], DBDMDB[7], and DBαMDB[7] agglomeration experiments were performed to better understand the photophysical characteristics of these molecules and to determine whether their photophysical properties in the agglomerated state and the solid state differ. The agglomeration study of DBDB[7], DBDMDB[7], and DBαMDB[7] in THF/water reveals that λ_{abs}, λ_{fl}, and ε in a 90% water suspension were similar to those in dilute THF solutions. However, for the aggregates in 70 or 80% water suspensions, large blue-shifts in λ_{fl} (particularly for DBαMDB[7]) and decreases in ε were observed, possibly owing to differences in the molecular conformations taken compared to those in dilute THF solution or the solid state (Figures S11–13, Tables S1–3).

Photophysical measurement of powdered DBαMDB[7] was performed (Figure S6). λ_{fl} and Φ_{solid} were similar before and after grinding, revealing that DBαMDB[**7**] is not a mechanochromic dye.[25]

5DBαMDB[7] exhibits emission characteristics similar to those of DBαMDB[7], whereas *t*BuDBαMDB[7], which has a bulky substituent, exhibits a high Φ_{solid} value (0.84), although $\lambda_{fl,solid}$ for this molecule is approximately 40 nm shorter than those for the other molecules due to conformational change. *t*BuDBαMDB[7] in the solid state and DBαMDB[7] in a 70–80% water suspension exhibit identical conformations, as their λ_{fl} values are similar. Steric hindrance caused by bulky substituents at the axial positions in *t*BuDBαMDB[7] results in a larger distance between the π-electron systems in the core than in the other DBDB[7]s. The introduction of substituents along the π-electron framework axis enables control over the crystal structure and fluorescence wavelength (Figure 4).

Although the conjugation lengths were shortened by the introduction of flexible bridges, it is apparent that this design strategy is advantageous for the development of AIEgens because DBDB[7]s exhibited almost no emission in THF but strong fluorescence in the solid state.

Category B

In a previous study,[15,16] DSB and PPB were found to form H-aggregates in the solid state. Compared to PPB in solution, solid-state PPB exhibits a longer $\lambda_{fl,solid}$ (Figure 3b) and a higher Φ_{solid} value.

The fact that the λ_{fl} and Φ_{fl} values of DSDMB and DBDB[6] are comparable to those of the DSBs implies that these molecules are likely to form H-aggregates, and the crystal structures of DSDMB and DBDB[6] are similar to that of DSB (Figures S21, S22, and S24). In DSB with methyl groups introduced at the lateral positions (DSDMB) or DSB with a

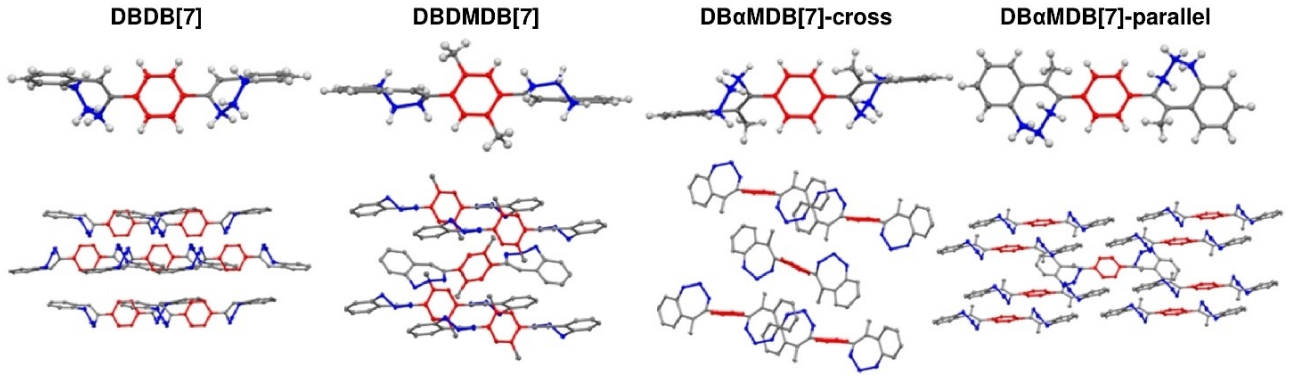

Figure 4. Single-molecule and crystal structures of DBDB[7], DBDMDB[7], DBαMDB[7]-cross, and DBαMDB[7]-parallel. The central benzene groups are shown in red, and the bridging groups are shown in blue.

highly planar six-membered-ring core (DBDB[6]), monomeric emission is unfavorable in the solid state, and in solution.

Single-crystal X-ray structure analysis

We analyzed the relationships between the photophysical properties and crystal structure among the investigated dyes.

Category A

The torsion angles between the C=C bonds and the central and outer benzene rings are ϕ_i and ϕ_o, respectively, as shown in Figure 5.

In DSB, the central and outer benzene rings occupy almost parallel planes. Conversely, DBDB[7] and DBDMDB[7] have large, twisted structures. The difference between ϕ_i and ϕ_o in DBDB[7] is only 7–9°; thus, the central and outer benzene rings are twisted to the same degree with respect to the double bond. DBDB[7] exists as one of two structures with different bridge configurations, and the two crystal structures are enantiomeric. In DBDMDB[7], ϕ_i is approximately 74° larger than ϕ_o, indicating that the central benzene ring is more twisted with respect to the double bond, compared to the outer benzene ring. DBαMDB[7] was dissolved in a hexane/dichloromethane mixture, and then the solution was gradually evaporated under atmospheric conditions to yield two types of single crystals: a cross type, with twisted central and outer benzene rings, and a parallel type, with almost no twisting (Figure 5). In both structures, the magnitudes of ϕ_o and ϕ_i are similar, and the central and outer benzene rings are twisted equally with respect to the bridging double bond. The λ_{fl} and Φ values of the two DBαMDB[7]-cross/parallel single crystals are shown in Figure 6.

In DBDB[7], DBDMDB[7], and DBαMDB[7], the benzene rings of adjacent overlapping molecules are almost orthogonal; thus, the electronic interactions are negligible. These three molecules exhibit solid-state monomeric emission. The molecular structure is probably similar to that in dilute THF solution, as their fluorescence properties in dilute THF solution and the solid state are similar.

In the case of DBαMDB[7], the molecular conformation can be controlled by recrystallization, and the conjugation length and luminescence properties of the chromophore can therefore be manipulated. Moreover, the λ_{fl} values of the DBαMDB[7] aggregate in a 70% water suspension and the DBαMDB[7]-parallel crystal were shown to be similar, indicating that these conformations are the same.

Finally, in terms of the molecular densities and occupancies, no difference was observed between the DSBs and DBDB[7]s (Table S6). Introducing a flexible bridging structure into the π-framework results in a different crystal, but the free volume is not increased.

The molecular structure of 5DBαMDB[7] was similar to that of DBαMDB[7]-cross, and that of *t*BuDBαMDB[7] was identical to that of DBαMDB[7]-parallel (Figure S20). For *t*BuDBαMDB[7], the distance between the benzene rings in adjacent molecules that overlapped in-phase was approximately 1.1 Å longer than that for DBαMDB[7]-parallel. We were not able to analyze the fluorescence properties of the DBαMDB[7]s in detail because

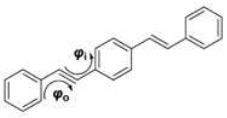

Entry	φ_o [°]	φ_i [°]
DSB	3.11 to 6.74	-8.72 to -2.68
DSDMB	9.45 4.13	16.11 23.47
PPB	31.77 30.72	-36.79 -34.19
DBDB[6]	11.36	-12.83
DBDB[7]	43.19 42.56	36.48 33.95
DBDMDB[7]	19.74	94.10
DBαMDB[7]-cross	42.79	48.10
DBαMDB[7]-parallel	50.40	-49.93

Figure 5. a) Definitions of ϕ_o and ϕ_i. b) Torsion angles of DBDB[7], DBDMDB[7], DBαMDB[7]-cross, and DBαMDB[7]-parallel.

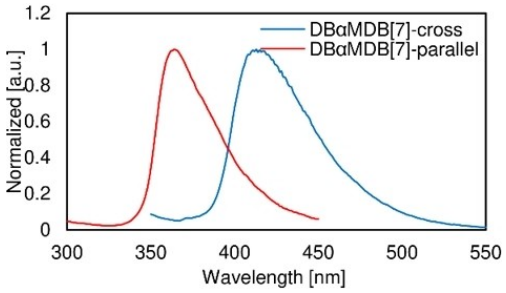

Entry	λ_{fl} [nm]	Φ [-]
DBαMDB[7]-cross	413	>0.99
DBαMDB[7]-parallel	364	0.84

Figure 6. Fluorescence spectra, λ_{fl}, and Φ of DBαMDB[7]-cross and DBαMDB[7]-parallel.

they exhibited no fluorescence in dilute THF solutions (AIE). However, these molecules are expected to exhibit monomeric fluorescence in the solid state, based on their Φ_{solid} and τ_{solid} values and crystal structures.[26]

Category B

Each molecule is highly planar, and DSB, PPB, and DBDB[6] adopt edge-to-face herringbone structures. The intermolecular distances between the chromophores (d_{chr}, Figure 7c) of DSB and DBDB[6] are 3.6 Å, whereas that of PPB is 3.7 Å. We define the tilt angle between the central and outer benzenes in adjacent molecules as α and β, respectively (Figure 7a). The magnitudes of α follow the order DBDB[6] > PPB > DSB, whereas those of β follow PPB > DSB > DBDB[6] (Figure 7b). In PPB, the electronic interactions are weak because the molecule exhibits a d_{chr} value larger than those of the other compounds, and α and β are $>70°$, suggesting large dihedral angles between adjacent molecules. Thus, the quantum yield of PPB is higher than those of the other DSBs. Conversely, DSDMB adopts a face-to-face zigzag column structure. In DSDMB, the d_{chr} value is 3.7 Å, which is the same as that of PPB, but stronger electronic interactions exist compared to those of PPB owing to the face-to-face structure, which might explain its low Φ_{solid} value.

DBDB[7] has unique crystal structures differing from those of any DSB derivatives, and exhibits many excellent characteristics. The introduction of flexible cyclic structures into π-cores contributes to diversity in crystal chemistry.

Theoretical study

We calculated the transition from the ground to the excited states of a single molecule with the configuration it takes in a single crystal using time-dependent self-consistent field theory at the ωB97XD/6-311G (d,p) level of theory. The calculated absorption wavelengths in the solid state are similar to the experimental values (Table S10). It is challenging to precisely assess the absorption wavelengths and molecular packing structures in the solid state using low-resolution diffuse-reflection spectra or these calculations. Therefore, herein we present a qualitative discussion of the photophysical property trends. Each of the compounds exhibited an $S_o \rightarrow S_1$ transition in which the highest occupied molecular orbital (HOMO)–lowest unoccupied molecular orbital (LUMO) transition was dominant (Table S10). The HOMO and LUMO electron cloud distributions and energy levels are shown in Figures S31 and S32 as well as Table S11. In DBDMDB[7], π-conjugation is localized and not extended. In contrast, in the other compounds, π-conjugation is extended over the entire molecule. Because ϕ_i of DBDMDB[7] is $>90°$, the π-conjugation is localized within the outer rings. Considering the HOMO and LUMO energies of all the compounds with respect to those of DSB, the HOMO energies are within ± 0.4 eV but the LUMO energies differ by up to 1.5 eV. The HOMO energy levels of DBαMDB[7]-cross and DBαMDB[7]-parallel, in particular, are similar, although their molecular structures differ considerably.

We calculated the overlap between the natural bond orbitals (NBOs) of adjacent molecules for the DSBs, DBDB[7], DBDMDB[7], and DBαMDB[7]-cross/parallel in single crystals at the ωB97X/6-311G(2d,2p) level of theory (Figures S33–S39). We analyzed only the overlap between occupied and unoccupied C=C bonding orbital of adjacent molecules because our focus was the molecular light-emitting behaviors in the solid state. Overlap between the NBOs in DSDMB was observed, but in DBDMDB[7], with the introduction of the bridging structure, NBO overlap was not observed. The NBO overlap of DBαMDB[7]-parallel is 0.49 kcal mol^{-1} less than that of PPB; conversely, that of DBDB[7] is 0.79 kcal mol^{-1} greater than that of DSB, and that of DBαMDB[7]-cross is 0.63 kcal mol^{-1} greater than that of PPB.

These results are not in accordance with the results of our photophysical study, which indicate that there is little electronic interaction between individual DBDB[7] molecules. However, NBO analyses evaluate the states of bonding orbitals isolated from the stabilizing structure of the π-conjugated system. Therefore, it is reasonable to suggest that the DBDB[7] molecules exist in unique crystal structures with few intramolecular electronic interactions, despite the close proximity of their adjacent π-conjugated planes.

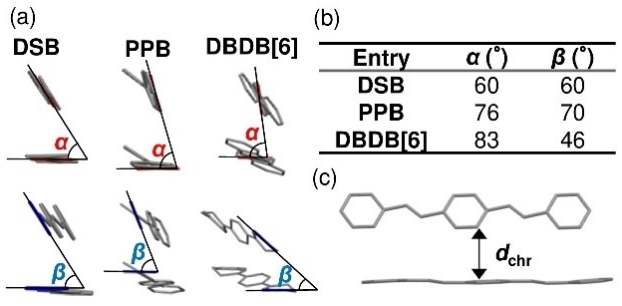

Entry	α (°)	β (°)
DSB	60	60
PPB	76	70
DBDB[6]	83	46

Figure 7. a) Arrangements of adjacent DSB,[14] PPB,[15] and DBDB[6] molecules in the solid state. The angles between the central (top row, α) and outer (bottom row, β) benzene rings are defined. b) Values of α and β for each compound. c) Definition of d_{chr}.

Conclusion

We have successfully synthesized bridged DSBs (DBDB[7]s), and crystal structures with compact packing, and solid-state monomeric fluorescence spectra similar to the dilute-solution fluorescence spectra were obtained. Unlike conventional design methods based on the use of bulky functional groups or capsules to isolate dyes, introducing small functional groups (flexible propylene bridges) to a π-conjugated system yielded monomeric emission in the solid state. The π-distortion and appropriate degree of steric hindrance generated by the flexible propylene bridges enabled the DBDB[7]s to form compact crystal structures with few intermolecular electronic interactions. The DBDB[7]s also possess the following valuable characteristics: 1) AIE character ($\Phi_{solid} > 0.80$); 2) low melting

points (Table S7) and good processability because they can adopt many conformations owing to their flexible cyclic structures; and 3) they are not mechanochromic. The fact that they are not mechanochromic means that these dyes have no limitations in terms of the processing methods that can be used in applications, and hence they can be incorporated into materials and devices. In other words, their application performance is, to a certain extent, independent of the environment. These unique properties suggest that the DBDB[7] molecules will contribute to future material design strategies. For example, a desired luminescence color can be generated by arranging multiple dyes with different luminescence wavelengths without them interacting with each other. The crystal structure obtained by introducing flexible cyclic structures to π-cores will depend on the selected π-electron molecule. This strategy dramatically expands the diversity of crystal structure fabrication approaches.

We plan to introduce alkylene bridges to various skeletons and further study the crystal chemistry of this class of molecules in the future. Development of the flexible-alkylene-bridge concept should reveal novel functions for materials based on hardly soluble rigid-rod π-conjugated molecules and polymers.[27] For these rod-shaped molecules, there is a trade-off between improving the processability and molecular alignment; this is an obstacle to improving device performance that we are currently attempting to resolve.

Experimental Section

Measurement methods of photophysical properties: UV-Vis spectra were recorded on a JASCO V-670 UV-vis spectrophotometer, and fluorescence spectra were recorded on a JASCO FP-6500 spectrofluorometer. The wavelengths obtained by the fluorescence spectrometer were converted to wavenumber using the equation $I(\tilde{\nu}) = \lambda^2 I(\lambda)^4$. Absolute quantum yields were measured by a Hamamatsu Photonics Quantaurus QY apparatus.

All photophysical measurements were performed using dilute solutions with optical densities (ODs) around 0.1 at the maximum absorption wavelength in 1 cm path length quartz cells at room temperature (298 K). In addition, all sample solutions were deaerated by bubbling with argon gas for 15 min prior to the quantum yield.

Emission lifetimes were obtained using a Horiba FluoroCube time-correlated single-photon counting system. The excitation light sources were LED pulse lamps (NanoLED, 269 and 379 nm). The solution samples were dissolved in THF and purged with argon for 20 min before lifetime measurements. In all samples, the time-to-amplitude converter ranges were 50 ns, and the amounts of counts were 10000. Reptation rates were 1 MHz in solution samples and 100 kHz in solid samples.

Diffuse-reflectance spectra were recorded on a JASCO FP-6500 spectrofluorometer equipped with an integration sphere detector. Thus, the experimental error arising from the fluorescence, typically encountered with diffuse-reflectance spectrometers producing polychromatic outgoing light, was avoided. Samples and references were charged in a JASCO powder sample cell to obtain a sufficiently thick powder layer. Just before each measurement, the synchronous spectrum of the NaBr powder was measured as a reflectance spectrum of a standard reference $r_{standard}(\lambda)$. Then, a reflectance spectrum of each sample $r_{sample}(\lambda)$ was obtained following the same procedure. In addition to neat powder samples, the spectra of samples adsorbed on the NaBr powder were measured at a concentration of 1.0×10^{-3} M. The obtained reflectance spectra $r_{sample}(\lambda)$ and $r_{standard}(\lambda)$ were converted to Kubelka–Munk functions $f(r_\infty)$ by using the following equation:

$$f(r_\infty) = \frac{(1 - r_\infty(\lambda))^2}{2r_\infty(\lambda)}, \text{ where } r_\infty(\lambda) = \frac{r_{sample}(\lambda)}{r_{standard}(\lambda)}$$

All diffuse-reflectance spectra are displayed at plots of the Kubelka-Munk functions, i.e., $f(r_\infty)$ as a function of the wavelength, λ.

X-ray crystallographic data: Deposition Numbers 2168494 (for DSDMB), 2168495 (for DBDB[6]), 2168496 (for DBDB[7]), 2168497 (for DBDMDB[7]), 2168498 (for DBαMDB[7]-cross), 2168499 (for DBαMDB[7]-parallel), 2168500 (5DBαMDB[7]), and 2168501 (for *t*BuDBαMDB[7]) contain the supplementary crystallographic data for this paper. These data are provided free of charge by the joint Cambridge Crystallographic Data Centre and Fachinformationszentrum Karlsruhe Access Structures service.

Synthesis of DBDB[7]s (Scheme 1)

*1-Methylene-1,2,3,4-tetrahydronaphthalene (**7a**)*: Methyltriphenylphosphonium bromide (8.0 g, 22.3 mmol) was dissolved in THF (50 mL) under argon and stirred at 0 °C. Potassium *tert*-butoxide (1.7 g, 22.1 mmol), and α-tetralone (**6**, 1.99 mL, 15.0 mmol) were added to the mixture and stirred at room temperature for 1 h. Saturated aqueous NH_4Cl was added, and the mixture was extracted with ethyl acetate. The organic layer was washed with water three times, dried over $MgSO_4$, filtered, and evaporated under reduced pressure to give a residue. The residue was chromatographed over silica gel, eluting with hexane/dichloromethane (3:1, *v*/*v*) to give crude **7a** as colorless oil. Yield: 85%; ^{1}H NMR (500 MHz, $CDCl_3$): $\delta = 7.65$ (d, $J = 7.3$ Hz, 1H), 7.18–7.13 (m, 2H), 7.10 (d, $J = 7.3$ Hz, 1H), 5.48 (s, 1H), 4.95 (s, 1H), 2.85 (t, $J = 6.1$ Hz, 2H), 2.55 (t, $J = 5.8$ Hz, 2H), 1.91–1.86 (m, 2H; Figure S49).

*1-Ethylidene-1,2,3,4-tetrahydronaphthalene (**7b**)*: Following a similar procedure used for the synthesis of **7b** from ethyltriphenylphosphonium Iodide (6.16 g, 14.7 mmol) and α-tetralone (**6**, 1.33 mL, 10.0 mmol) stirred at room temperature for 4 h, chromatography over silica gel, eluting with hexane/dichloromethane (4:1, *v*/*v*) gave crude **7b** as a colorless oil. Yield:

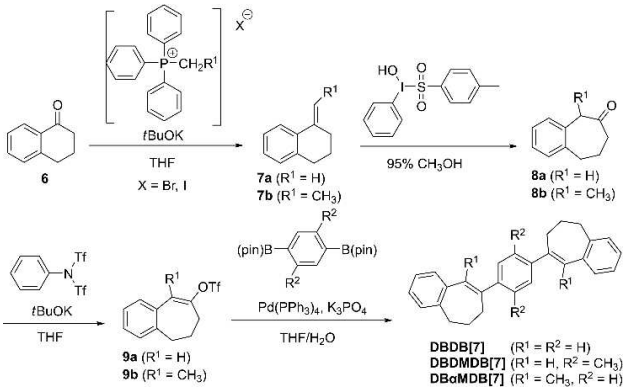

Scheme 1. Synthesis of DBDB[**7**], DBDMDB[**7**], and DBαMDB[**7**].

97%;[1]H NMR (399 MHz, $CDCl_3$): $\delta = 7.57–7.55$ (m, 1H), 7.42 (dt, $J =$ 8.5, 3.4 Hz, 0H), 7.18–7.07 (m, 3H), 6.14–6.08 (m, 1H), 5.57 (q, $J =$ 7.3 Hz, 0H), 2.83 (t, $J = 6.6$ Hz, 1H), 2.76 (t, $J = 6.2$ Hz, 1H), 2.50 (t, $J = 6.4$ Hz, 1H), 2.43–2.39 (m, 1H), 1.93–1.79 (m, 5H; Figure S50; **7b** was a mixture of *E* and *Z* configurations).

*5,7,8,9-Tetrahydro-6*H*-benzo[7]annulen-6-one (**8a**)*:[18] **7a** (1.83 g, 12.7 mmol) was dissolved in 95% methanol (60 mL), and [hydroxy(tosyloxy)iodo]benzene (5.01 g, 12.8 mmol) was added. The solid dissolved evolution of heat rapidly to a yellow solution. The solution was stirred at room temperature for 20 min, and the solvent was removed in vacuo. Dichloromethane and water were added, and the mixture was extracted with dichloromethane. The organic layer was washed with water and brine three times, dried over $MgSO_4$, filtered, and evaporated under reduced pressure to give a residue. The residue was chromatographed over silica gel, eluting with hexane/ethyl acetate (3:1, *v/v*) to give crude **8a** as a colorless oil. Yield: 84%; [1]H NMR (500 MHz, $CDCl_3$): $\delta = 7.22–7.14$ (m, 4H), 3.73 (s, 2H), 2.95 (t, $J = 6.3$ Hz, 2H), 2.57 (t, $J = 6.9$ Hz, 2H), 2.02–1.97 (m, 2H; Figure S51).

*5-Methyl-5,7,8,9-tetrahydro-6*H*-benzo[7]annulen-6-one (**8b**)*:[18] Following a similar procedure used for the synthesis of **8a** from **7b** (1.36 g, 8.6 mmol), chromatography over silica gel, eluting with hexane/ethyl acetate (3:1, *v/v*) gave crude **8b** as a colorless oil. Yield: 69%;[1]H NMR (399 MHz, $CDCl_3$): $\delta = 7.24–7.18$ (m, 3H), 7.16–7.10 (m, 1H), 3.88 (q, $J = 7.2$ Hz, 1H), 2.97 (qd, $J = 7.3$, 4.6 Hz, 1H), 2.87–2.80 (m, 1H), 2.68–2.63 (m, 1H), 2.48 (qd, $J = 5.9$, 4.2 Hz, 1H), 2.09–2.04 (m, 1H), 1.98–1.87 (m, 1H), 1.45 (d, $J = 6.9$ Hz, 3H; Figure S52. The compound was a 11:5 mixture of ketone and acetal).

*6,7-Dihydro-5*H*-benzo[7]annulen-8-yl trifluoromethanesulfonate (**9a**)*: **8a** (1.70 g, 10.6 mmol) was dissolved in THF (30 mL) under argon. The reaction mixture was cooled to −20 °C, and potassium tert-butoxide (1.58 g, 14.1 mmol) was added to the mixture and stirred at 0 °C for 1 h. The mixture was cooled to −20 °C, and *N*-phenylbis(trifluoromethanesulfonimide) (4.95 g, 14.1 mmol) was added to the mixture and stirred at −20 °C for 1 h, and then stirred at 0 °C for 4 h. Water was added, and the mixture was extracted with ethyl acetate. The organic layer was washed with water and saturated with aqueous NaHCO3, dried over MgSO4, filtered, and evaporated under reduced pressure to give a residue. The residue was chromatographed over silica gel, eluting with hexane/ethyl acetate (6:1, *v/v*) to give crude **9a** as a colorless oil. Yield: 93%; [1]H NMR (500 MHz, $CDCl_3$): $\delta = 7.21–7.16$ (m, 3H), 7.11 (t, $J = 4.1$ Hz, 1H), 6.59 (s, 1H), 2.89 (t, $J = 4.9$ Hz, 2H), 2.79 (t, $J = 6.6$ Hz, 2H), 2.02–1.97 (m, 2H; Figure S53. (The compound was a 5:1 mixture of **9a** and N-phenylbis(trifluoromethanesulfonimide).

*9-Methyl-6,7-dihydro-5*H*-benzo[7]annulen-8-yl trifluoromethanesulfonate (**9b**)*: Following a similar procedure used for the synthesis of **9a** from **8b** (1.16 g, the amount of ketone = 4.4 mmol), chromatography over silica gel, eluting with hexane/ethyl acetate (6:1, *v/v*), gave crude **9b** as a colorless oil. Yield: 41%; [1]H NMR (399 MHz, $CDCl_3$): $\delta = 7.32–7.28$ (m, 2H), 7.24–7.21 (m, 2H), 2.69 (t, J = 6.6 Hz, 2H), 2.32–2.22 (m, 4H), 2.17 (s, 3H) (Figure S54).

*1,4-Bis(6,7-dihydro-5*H*-benzo[7]annulen-8-yl)benzene (DBDB[7])*: A mixture of **9a** (0.90 g, 3.1 mmol), 1,4-benzendiboronic acid bis(pinacol) ester (0.47 g, 1.4 mmol), K_3PO_4 (2.06 g, 9.7 mmol), and $Pd(PPh_3)_4$ (0.18 g, 0.16 mmol) was dissolved in THF/water (5:1, *v/v*; 15 mL) under argon. The reaction mixture was refluxed at 60 °C overnight and then cooled to room temperature. The organic layer was washed with water three times, dried over $MgSO_4$, filtered, and evaporated under reduced pressure to give a residue. The residue was chromatographed over silica gel, eluting with hexane/dichloromethane (9:1, *v/v*), and recrystallizing from hexane/dichloromethane (3:1, *v/v*) to give DBDB[**7**] as a yellowish solid. Yield: 17%; Mp: 181.2 °C; [1]H NMR (399 MHz, $CDCl_3$): $\delta = 7.52$ (s, 4H), 7.26–7.21 (m, 4H), 7.19 (d, $J = 6.4$ Hz, 2H), 7.17–7.13 (m, 2H), 6.86 (s, 2H), 2.83 (t, $J = 6.2$ Hz, 4H), 2.67 (t, $J =$ 6.9 Hz, 4H), 2.27–2.21 (m, 4H) (Figure S55); [13]C NMR (100 MHz, $CDCl_3$): $\delta = 142.9$, 142.5, 141.4, 137.6, 130.5, 129.1, 128.5, 126.7, 126.2, 126.1, 34.4, 32.4, 30.9 (Figure S56); HRMS (EI) calcd for $C_{28}H_{26}$: 362.2035; found: 362.2028 (Figure S73).

*8,8′-(2,5-Dimethyl-1,4-phenylene)bis(6,7-dihydro-5*H*-benzo[7]annulene) (DBDMDB[7])*: Following a similar procedure used for the synthesis of DBDB[**6**] from **9a** (0.90 g, 3.1 mmol) and 2,5-dimethyl-1,4-dibenzenediboronic acid bis(pinacol) ester (0.50 g, 1.4 mmol), refluxed at 50 °C overnight, chromatography over silica gel, eluting with hexane/dichloromethane (9:1, *v/v*), and recrystallization from hexane/dichloromethane (2:1, *v/v*) gave DBDMDB[**7**] as a colorless solid. Yield: 55%; Mp: 156.9 °C; [1]H NMR (399 MHz, $CDCl_3$): $\delta = 7.21–7.11$ (m, 8H), 7.06 (s, 2H), 6.41 (s, 2H), 2.94–2.91 (m, 4H), 2.55 (t, $J = 6.4$ Hz, 4H), 2.34 (s, 6H), 2.20–2.13 (m, 4H) (Figure S57); [13]C NMR (100 MHz, $CDCl_3$): $\delta =$ 144.4, 144.3, 141.4, 136.9, 131.9, 130.7, 130.3, 129.9, 129.2, 126.6, 126.1, 36.2, 35.4, 29.3, 19.6 (Figure S58); HRMS (EI) calcd for $C_{30}H_{30}$: 390.2348; found: 390.2351 (Figure S74).

*1,4-Bis(9-methyl-6,7-dihydro-5*H*-benzo[7]annulen-8-yl)benzene (DBαMDB[7])*: Following a similar procedure used for the synthesis of DBDB[**6**] from **9b** (0.31 g, 1.0 mmol) refluxed at 50 °C for 1.5 h, chromatography over silica gel, eluting with hexane/dichloromethane (9:1, *v/v*), and recrystallization from methanol/dichloromethane (3:1, *v/v*) gave DBαMDB[**7**] as a colorless solid. Yield: 49%; Mp: 163.3 °C; [1]H NMR (399 MHz, $CDCl_3$): $\delta = 7.37$ (dd, J = 7.8, 0.9 Hz, 2H), 7.31–7.27 (m, 6H), 7.23 (dd, $J = 7.3$, 1.8 Hz, 2H), 7.19 (td, $J = 7.1$, 1.4 Hz, 2H), 2.71 (t, $J = 6.9$ Hz, 4H), 2.20 (m, 8H), 2.10 (s, 6H) (Figure S59); [13]C NMR (100 MHz, $CDCl_3$): $\delta = 143.6$, 142.0, 140.3, 137.9, 131.8, 128.6, 128.3, 126.6, 126.2, 34.7, 32.9, 32.2, 20.1 (Figure S60); HRMS (EI) calcd for $C_{30}H_{30}$: 390.2348; found: 390.2350 (Figure S75).

Acknowledgements

The authors thank Masato Koizumi (Materials Analysis Division, Tokyo Institute of Technology) for the HRMS measurements. This research was supported in part by MEXT/JSPS KAKENHI grants 18H02045 and 17H05145 (awarded to G. K.), 21K05165 (awarded to R. G.), by JSPS fellowship 21J01295 (awarded to N. S.), and by funding from the Toshiaki Ogasawara Memorial Foundation and the Murata Science Foundation (grants awarded to G. K.). This research was supported by the Research Program of "Network Joint Research Center for Materials and Devices".

Conflict of Interest

The authors declare no conflict of interest.

Data Availability Statement

The data that support the findings of this study are available in the supplementary material of this article.

Keywords: aggregation-induced emission · crystal engineering · distyrylbenzene · organic light-emitting devices (OLEDs) · solid state fluorescence

[1] a) H. Sasabe, J. Kido, *J. Mater. Chem. C* **2013**, *1*, 1699–1707; b) G. Hong, X. Gan, C. Leonhardt, Z. Zhang, J. Sibert, J. M. Busch, S. Bräse, *Adv. Mater.* **2021**, *33*, 2005630; c) J. Yang, M. Fang, Z. Li, *Aggregate* **2020**, *1*, 6–18; d) S. Oda, W. Kumano, T. Hama, R. Kawasumi, K. Yoshiura, T. Hatakeyama, *Angew. Chem. Int. Ed.* **2021**, *60*, 2882–2886; *Angew. Chem.* **2021**, *133*, 2918–2922; e) U. Balijapalli, R. Nagata, N. Yamada, H. Nakanotani, M. Tanaka, A. D'Aléo, V. Placide, M. Mamada, Y. Tsuchiya, C. Adachi, *Angew. Chem. Int. Ed.* **2021**, *60*, 8477–8482; f) M. Shimizu, T. Sakurai, *Aggregate* **2022**, *3*, e144; g) I. S. Park, H. Min, T. Yasuda, *Aggregate* **2021**, *2*, e96; h) J. Gierschner, J. Q. Shi, B. Milian-Medina, D. Roca-Sanjuan, S. Varghese, S. Park, *Adv. Opt. Mater.* **2021**, *9*, 2002251; i) F. Ito, R. Naganawa, Y. Fujimoto, M. Takimoto, Y. Mochiduki, S. Katsumi, *ChemPhysChem* **2021**, *22*, 1662–1666; j) Y. Shoji, N. Tanaka, Y. Ikabata, H. Sakai, T. Hasobe, N. Koch, H. Nakai, T. Fukushima, *Angew. Chem. Int. Ed.* **2022**, *61*, e202113549; k) Y. Matsui, Y. Yokoyama, T. Ogaki, K. Ishiharaguchi, A. Niwa, E. Ohta, M. Saigo, K. Miyata, K. Onda, H. Naito, H. Ikeda, *J. Mater. Chem. C* **2022**, *10*, 4607–4613; l) M. Shimizu, K. Nishimura, R. Hirakawa, T. Sakurai, *Chem. Eur. J.* **2021**, *27*, 1626–1637; m) T. Kusamoto, S. Kimura, *Chem. Lett.* **2021**, *50*, 1445–1459; Y. Takeda, P. Data, S. Minakata, *Chem. Commun.* **2020**, *56*, 8884–8894; n) Y. Niko, S. Sasaki, K. Narushima, D. K. Sharma, M. Vacha, G. Konishi, *J. Org. Chem.* **2015**, *80*, 10794–10805.

[2] a) W. Wang, *Chem. Soc. Rev.* **2018**, *47*, 2485–2508; b) C. Severi, S. Lahtinen, J. Rosenberg, A. Reisch, T. Soukka, A. S. Klymchenko, *Aggregate* **2022**, *3*, e130; c) X. Liu, Y. Duan, B. Liu, *Aggregate* **2021**, *2*, 4–19; d) B. Andreiuk, I. O. Aparin, A. Reisch, A. S. Klymchenko, *Chem. Eur. J.* **2021**, *27*, 12877–12883.

[3] a) Y. Sang, J. Han, T. Zhao, P. Duan, M. Liu, *Adv. Mater.* **2020**, *32*, 1900110; b) E. M. Sanchez-Carnerero, A. R. Agarrabeitia, F. Moreno, B. L. Maroto, G. Muller, M. J. Ortiz, S. de la Moya, *Chem. Eur. J.* **2015**, *39*, 13488–13500; c) C. Maeda, S. Nomoto, K. Takaishi, T. Ema, *Chem. Eur. J.* **2020**, *26*, 13016–13021; d) L. Arrico, L. Di Bari, F. Zinna, *Chem. Eur. J.* **2021**, *27*, 2920–2934; e) C. Zhang, S. Li, X.-Y. Dong, S.-Q. Zang, *Aggregate* **2021**, *2*, e48; f) H. Kubo, D. Shimizu, T. Hirose, K. Matsuda, *Org. Lett.* **2020**, *22*, 9276–9281.

[4] a) A. S. Klymchenko, *Acc. Chem. Res.* **2017**, *50*, 366–375; b) X. Cai, B. Liu, *Angew. Chem. Int. Ed.* **2020**, *59*, 9868–9886; *Angew. Chem.* **2020**, *132*, 9952–9970; c) Y. Niko, P. Didier, I. Mely, G. Konishi, A. S. Klymchenko, *Sci. Rep.* **2016**, *6*, 18870; d) Y. Niko, S. Kawauchi, G. Konishi, *Chem. Eur. J.* **2013**, *19*, 9760–9765; e) Ž. Ban, S. Griesbeck, S. Tomić, J. Nitsch, T. B. Marder, I. Piantanida, *Chem. Eur. J.* **2020**, *26*, 2195–2203; f) Y. Niko, H. Moritomo, H. Sugihara, Y. Suzuki, J. Kawamata, G. Konishi, *J. Mater. Chem. B* **2016**, *4*, 2731–2743; g) S. Sasaki, G. P. C. Drummen, G. Konishi, *J. Mater. Chem. C* **2016**, *4*, 2731–2743; h) G. K. Kole, M. Koscak, A. Amar, D. Majhen, K. Bozinovic, Z. Brkljaca, M. Ferger, E. Michail, S. Lorenzen, A. Friedrich, I. Krummenacher, M. Moos, H. Braunschweig, A. Boucekkine, C. Lambert, J. F. Halet, I. Piantanida, K. Muller-Buschbaum, T. B. Marder, *Chem. Eur. J.* **2022**, *28*, e202200753; i) M. Kang, Z. Zhang, N. Song, M. Li, P. Sun, X. Chen, D. Wang, B. Z. Tang, *Aggregate* **2020**, *1*, 80–106; j) Y. Niko, S. Sasaki, S. Kawauchi, K. Tokumaru, G. Konishi, *Chem. Asian J.* **2014**, *9*, 1797–1807; k) Y. Niko, Y. Cho, S. Kawauchi, G. Konishi, *RSC Adv.* **2014**, *4*, 36480–36484.

[5] a) A. J. C. Kuehne, M. C. Gather, *Chem. Rev.* **2016**, *116*, 12823–12864; b) M. Uchimura, Y. Watanabe, F. Araoka, J. Watanabe, H. Takezoe, G. Konishi, *Adv. Mater.* **2010**, *22*, 4473–4478; c) Y. Oyama, M. Mamada, A. Shukla, E. G. Moore, S.-C. Lo, E. B. Namdas, C. Adachi, *ACS Materials Lett.* **2020**, *2*, 161–167.

[6] a) M. K. Bera, P. Pal, S. Malik, *J. Mater. Chem. C* **2020**, *8*, 788–802; b) S. D. Xu, T. T. Liu, Y. X. Mu, Y. F. Wang, Z. G. Chi, C. C. Lo, S. W. Liu, Y. Zhang, A. Lien, J. R. Xu, *Angew. Chem. Int. Ed.* **2015**, *54*, 874–878; *Angew. Chem.* **2015**, *127*, 888–892; c) D. Yan, D. G. Evans, *Mater. Horiz.* **2014**, *1*, 46–57; d) G. Fan, D. Yan, *Sci. Rep.* **2014**, *4*, 4933; e) B. Zhou, Q. Zhao, L. Tang, D. Yan, *Chem. Commun.* **2020**, *56*, 7698–7701.

[7] a) E. E. Jelley, *Nature* **1936**, *138*, 1009; b) F. Würthner, T. E. Kaiser, C. R. Saha-Möller, *Angew. Chem. Int. Ed.* **2011**, *50*, 3376–3410; *Angew. Chem.* **2011**, *123*, 3436–3473; c) B. K. An, J. Gierschner, S. Y. Park, *Acc. Chem. Res.* **2012**, *45*, 544–554; d) J. L. Bricks, Y. L. Slominskii, I. D. Panas, A. P. Demchenko, *Methods Appl. Fluoresc.* **2018**, *6*, 012001; e) Y. Kotani, H. Yasuda, K. Higashiguchi, K. Matsuda, *Chem. Eur. J.* **2021**, *27*, 11158–11166; f) A. C. B. Rodrigues, D. Wetterling, U. Scherf, J. S. Seixas de Melo, *Chem. Eur. J.* **2021**, *27*, 7826–7830; g) C. Ji, L. Lai, P. Li, Z. Wu, W. Cheng, M. Yin, *Aggregate* **2021**, *2*, e39.

[8] a) C.-H. Zhao, A. Wakamiya, Y. Inukai, S. Yamaguchi, *J. Am. Chem. Soc.* **2006**, *128*, 15934–15935; b) S. Masuo, H. Yoshikawa, T. Asahi, H. Masuhara, T. Sato, D.-L. Jiang, T. Aida, *J. Phys. Chem. B.* **2003**, *107*, 2471–2479; c) B. Sadowski, K. Hassasnein, B. Ventura, D. T. Gryko, *Org. Lett.* **2018**, *20*, 3183–3186; d) S. Hecht, J. M. J. Fréchet, *Angew. Chem. Int. Ed.* **2001**, *40*, 74–91; *Angew. Chem.* **2001**, *113*, 76–94.

[9] a) R. Huang, B. Liu, C. Wang, Y. Wang, H. Zhang, *J. Phys. Chem. C* **2018**, *122*, 10510–10518; b) Y. Shi, K. Wang, Y. Tsuchiya, W. Liu, T. Komino, X. Fan, D. Sun, G. Daiole, J. Chen, M. Zhang, C. Zheng, S. Xiong, X. Ou, J. Yu, J. Jie, C.-S. Lee, C. Adachi, X. Zhang, *Mater. Horiz.* **2020**, *7*, 2734–2740.

[10] a) Z. Zhao, H. Zhang, J. W. Y. Lam, B. Z. Tang, *Angew. Chem. Int. Ed.* **2020**, *59*, 9888–9907; *Angew. Chem.* **2020**, *132*, 9972–9993; b) S. Suzuki, S. Sasaki, A. S. Sairi, R. Iwai, B. Z. Tang, G. Konishi, *Angew. Chem. Int. Ed.* **2020**, *59*, 9856–9867; *Angew. Chem.* **2020**, *132*, 9940–9951; c) J. Ochi, K. Tanaka, Y. Chujo, *Angew. Chem. Int. Ed.* **2020**, *59*, 9841–9855; *Angew. Chem.* **2020**, *132*, 9925–9939; d) S. Sasaki, S. Suzuki, W. M. C. Sameera, K. Igawa, K. Morokuma, G. Konishi, *J. Am. Chem. Soc.* **2016**, *138*, 8194–8206; e) S. Sasaki, S. Suzuki, K. Igawa, K. Morokuma, G. Konishi, *J. Org. Chem.* **2017**, *82*, 6865–6873; f) L.-H. Wang, Y. Nagashima, M. Abekura, H. Uekusa, G. Konishi, K. Tanaka, *Chem. Eur. J.* **2022**, *28*, e202200064; g) S. Ito, R. Sekine, M. Munakata, M. Yamashita, T. Tachikawa, *Chem. Eur. J.* **2021**, *27*, 13982–13990; h) J. Rouillon, C. Monnereau, C. Andraud, *Chem. Eur. J.* **2021**, *27*, 8003–8007; i) K. Pauk, S. Lunak, A. Ruzicka, A. Markova, A. Mausova, M. Kratochvil, K. Melanova, M. Weiter, A. Imramovsky, M. Vala, *Chem. Eur. J.* **2021**, *27*, 4341–4348; j. Rouillon, C. Monnereau, C. Andraud, *Chem. Eur. J.* **2021**, *27*, 8003–8007; j) S. Sasaki, K. Igawa, G. Konishi, *J. Mater. Chem. C* **2015**, *3*, 5940–5950; k) Y. Arakawa, S. Sasaki, K. Igawa, M. Tokita, G. Konishi, H. Tsuji, *New J. Chem.* **2020**, *44*, 17531–17541; l) H. V. Miyagishi, H. Masai, J. Terao, *Chem. Eur. J.* **2022**, *28*, e202103175.

[11] A. Reisch, A. S. Klymchenko, *Small* **2016**, *12*, 1968–1992.

[12] D. Bialas, E. Kirchner, M. I. S. Röhr, F. Würthner, *J. Am. Chem. Soc.* **2021**, *143*, 4500–4518.

[13] J. Gierschner, S. Y. Park, *J. Mater. Chem. C* **2013**, *1*, 5818–5832.

[14] Other examples of highly emissive DSB derivatives in the solid state exist, based on cocrystal strategies - see, a) D, Yan, A, Delori, G. O. Lloyd, T. Friščić, G. M. Day, W. Jones, J. Lu, M. Wei, D. G. Evans, X. Duan, *Angew. Chem. Int. Ed.* **2011**, *50*, 12483–12486; *Angew. Chem.* **2011**, *123*, 12691–12694; b) D. Yan, W. Jones, G. Fan, M. Wei, D. G. Evans, *J. Mater. Chem. C.* **2013**, *1*, 4138–4145.

[15] S. Varghese, S. K. Park, S. Casado, R. C. Fischer, R. Resel, B. M–Medina, R. Wannemacher, S. Y. Park, J. Gierschner, *J. Phys. Chem. Lett.* **2013**, *4*, 10, 1597–1602.

[16] C. J. Bhongale, C. W. Chang, C.-S. Lee, E. W.-G. Diau, C.-S. Hsu, *J. Phys. Chem. B* **2005**, *109*, 13472–13482.

[17] Z. Yang, H. J. Geise, M. Mehbod, G. Dbrue, J. W. Visser, E. J. Sonneveld, L. Van't dack, R. Gijbels, *Syn. Met.* **1990**, *39*, 137–151.

[18] a) T. Ueda, H. Konishi, K. Manabe, *Org. Lett.* **2012**, *14*, 5370–5373; b) M. W. Justik, G. F. Koser, *Molecules* **2005**, *10*, 217–225.

[19] R. Iwai, S. Suzuki, S. Sasaki, A. S. Sairi, K. Igawa, T. Suenob, K. Morokuma, G. Konishi, *Angew. Chem. Int. Ed.* **2020**, *59*, 10566–10573; *Angew. Chem.* **2020**, *132*, 10653–10660.

[20] K. Kato, K. Takaba, S. Maki-Yonekura, N. Mitoma, Y. Nakanishi, T. Nishihara, T. Hatakeyama, T. Kawada, Y. Hijikata, J. Pirillo, L. T. Scott, K. Yonekura, Y. Segawa, K. Itami, *J. Am. Chem. Soc.* **2021**, *143*, 5465–5469.

[21] a) I. R. Marquez, S. C. Fernandez, A. Millan, A. G. Gampana, *Chem. Commun.* **2018**, *54*, 6705–6718; b) K. Kawai, K. Kato, L. Peng, Y. Segawa, L. T. Scott, K. Itami, *Org. Lett.* **2018**, *20*, 1932–1935.

[22] The non-radiative decays of the DBDB[**7**] molecules occur via a conical intersection (CI).[19] DBDB[**7**]s are not solvatochromic dyes (Figure S14 and Table S4). They consist of hydrocarbons, and their electronic states are not affected by solvent polarity.

[23] a) T. Tahara, H. Hamaguchi, *Chem. Phys. Lett.* **1994**, *217*, 369–374; b) K. Kokado, T. Machida, T. Iwasa, T. Taketsugu, K. Sada, *J. Phys. Chem. C* **2018**, *122*, 245–251.

[24] a) J. B. Birks, L. G. Christphorou, *Spectrochim. Acta* **1953**, *19*, 401–410; b) H. Liu, L. Yao, B. Li, X. Chen, Y. Gao, S. Zhang, W. Li, P. Lu, B. Yang, Y. Ma, *Chem. Commun.* **2016**, *52*, 7356–7359.

[25] The reasons for judging that DBαMDB[**7**] is not a mechanochromic dye are as follows: a) luminescence changes before and after grinding were not observed; b) although a very small difference in the luminescence

peak wavelength was apparently measured, it should be recalled that a commercially available fluorescence spectrometer possesses a measurement error of 3–5 nm, and hence the observed difference should be neglected.

[26] Determining whether organic dyes strictly exhibit monomeric emission is difficult; however, luminescence spectrum changes caused by an intermolecular electronic interaction should be observable. The photophysical properties of PMMA films doped with a DBDB[**7**] (0.1 wt%) were measured (Figures S15–S19 and Table S5), and λ_{abs} and λ_{fl} of almost all these films were similar to those in THF and the solid state, respectively.

[27] a) Z. Ding, D. Liu, K. Zhao, Y. Han, *Macromolecules* **2021**, *54*, 3907–3926; b) D. Khim, A. Luzio, G. Bonacchini, G. Pace, M.-J. Lee, Y.-Y. Noh, M. Caironi, *Adv. Mater.* **2018**, *30*, 1705463.

Manuscript received: June 19, 2022
Accepted manuscript online: July 11, 2022
Version of record online: July 28, 2022